

Magnetism of 3d Transition Metals and Magnetic Anisotropy of one-dimension Ni Chains on Au(110)-(1×2): A Noncollinear *ab-initio* Density-Functional-Theory Study

Wei Fan^a, Xin-Gao Gong^{b,a}

^a *Key Laboratory of Materials Physics, Institute of Solid State Physics, Chinese Academy of Sciences, 230031-Hefei, P. R. China*

^b *Department of Physics, Fudan University, 200433-Shanghai, P. R. China*

Abstract

Based on Density Functional Theory (DFT) with non-collinear-magnetism formulations, we have calculated the magnetism of single atom of 3d transition metals and the magnetic anisotropy of supported Ni chains on Au(110)-(1×2) surface. Our results show that surface relaxations enhance the orbital moments of left-end elements (Ti,V) and quench the orbital moments of right-end elements (Fe,Co,Ni) on the Au(110)-(1×2) surface. This is because Ti and V atoms raise their positions above the trough of the reconstructed Au(110) surface and Fe, Co, Ni atoms trap more deeply in the trough after the surface relaxations. From the study of magnetism of Ni one-dimensional atomic chains, their magnetic anisotropy are closely relate to their orbital quenching. The easy magnetized axis changes from the direction parallel to the chains to the direction perpendicular to the Ni chains when they absorb on the surface. These one-dimensional Ni chains in the trough of the reconstructed Au(110) surface have ferromagnetic order and are favored with chain-length less than 6.

Key words: Non-Collinear Density Functional Theory, Surface Magnetism, one-dimensional Magnetism, Magnetic Crystalline Anisotropy

PACS: 75.70.Ak, 75.30.Gw, 75.75.+a, 71.15.Mb

1 Introduction

The high-density magnetic recording and the memory devices require the strong magnetic anisotropy. The low-dimensional materials due to the reduced

dimensionality generally have a favorable direction and the physical properties along this direction are generally different from the other directions. Thus we have the most possibilities to find the strong magnetic anisotropy materials from these low-dimensional materials. On the other hand, the reduced dimensionality reduces the atomic coordination number and enhances the spin and orbital magnetic moments of the materials. Since the pioneering experiments for the magnetism of Fe strips on the W(110) and Cu(111) surfaces [1–4], the researches along this direction have been extended to others quasi-one-dimensional systems such as the monatomic magnetic chains on vicinal surface [5–7] and Co magnetic dot-chain on Ru(0001) surface [8]. The transition from in-plane to out-of-plane magnetic anisotropy had been found in Fe nano-structure when it is approach to one-dimensional limit [9]. Besides the celebrating properties such as the strong magnetic anisotropy, the enhanced spin and orbital moments, some new phenomena have been found, such as the temperature and time dependent magnetization [1,2] which make the realistic applications of these novel experimental devices face new serious problem such as the instability of magnetic structure.

It is valuable to investigate theoretically the magnetic stability of surface-supported novel structures [10]. Many theoretical and computational methods have been used to studied the magnetism of one-dimensional structure on surface such as the KKR [11–14], and TB-LMTO [15] and PAW methods [16, 17] based on Density Functional Theory, and the numerically tight-binding self-consistent calculation [18] and analytically tight-binding calculation [19]. Some common arguments have been found such as the enhancement of surface magnetism, the magnetic anisotropy are close related to the orbital moments and the spin-orbit coupling interaction (SOC).

The orbital polarization [20–22] can remedy the small orbital moments in the calculations of density functional theory to approach the experimental values, and especially reproduce the correct phase transition in Ce accompanying with the volume collapses [21]. The orbital polarization plays the opposite role to crystal field which quenches the orbital moment to small value in crystal due to the splitting of ground state energy levels. However there are still many contradictions among the already known theoretical results. The density functional calculations with OP (orbital polarization) + SOC (spin-orbit coupling) have given the correct orbital moments but too large MAE (Magnetic Anisotropy Energy) for tetragonal and cubic Ni. If the OP term switches off the theoretical value of the magnetic anisotropy energy is close its experimental values [23]. The magnetic anisotropy energy of CoPt calculated using the so-called c-RPA [24] are weakly dependent on the new introduced OP interaction. The magnetic anisotropy energies are surprisingly consistent with experiments even only under LSDA approximation without the OP effects. The orbital moments of transition metals are well consistent with experiments. This method has been combined with PAW method to calculate quasi-particle

spectrum of materials [25].

Based on Brook's theory, the magnetic anisotropy is induced by the spin-orbital interaction [26]. Although the orbital moments are underestimated, it's still valuable to study the magnetic anisotropy properties in the absence of (OP) orbital polarization term. Theoretical works based on Density Functional Theory have also discovered others interesting properties of surface supported magnetic chains. Such as in Ref. [17], the authors have studied the magnetism of the ultrathin wires of fifth and sixth row elements supported on Cu(117) and Ag(117) vicinal surfaces. They found that only metals with a half-filled d band are found to have magnetic order on Cu(117) surface, additionally the ferromagnetic order is energetically stable. On the contrary, on the Ag(117) surface, the anti-ferromagnetic order is stable. The magnetism of mono-atomic chain is strongly dependent on their local environment absorbed on the surfaces.

Besides the high-index vicinal surfaces such as Ag(117), the reconstructed Au(110)-(1 \times 2) surface decorated with one-dimensional troughs along the closed-packed A-[$\bar{1}\bar{1}0$] direction can be used as a template to grow one-dimensional nano-structure. Experimentally, the distribution of lengths of Ni chains shows that most Ni chains are short than 6 [27]. Our molecular simulation additionally shows that the lattice misfit between Ni chains and the Au substrate can induce the instability of Ni chains and makes them break into short segments [28].

In this work we study the magnetism of mono-atomic Ni chains supported on Au(110)-(1 \times 2) surface using the same theoretical method as in Ref. [17]. Our studies focus on the magnetic anisotropy of surface-supported magnetic atomic chains. We perform the non-collinear magnetic calculations including the spin-orbit coupling interaction but without orbital polarization interaction. We have calculated the magnetic anisotropy energies of the supported Ni chains and found an off-plane easy magnetization axis perpendicular to the chains and the surface. On the contrary, the easy magnetization axes of the free-standing Ni chains are parallel to these chains. The change of the easy magnetization axes of the surface-supported chains are also found in the others systems [18]. Our results also indicate the closed relationship between the magnetic anisotropy and the orbital magnetism.

The paper is arranged as follow. In the next section, we introduce the theoretical methods used in this paper. The third section will present the results for single 3d transition metal atoms absorbed on Au(110)-(1 \times 2) and Au(111) surface. The magnetism of a single magnetic atom on a surface is important to understand the magnetism of materials with more complex structures such as the one-dimensional nano-structure. The reduced dimensionality and coordination number for surface still enhance the magnetism of single absorbed

atoms [29–33]. The results of short one-dimensional mono-atomic Ni chains are included in the forth section. Our studies focus on the magnetic anisotropy of Ni mono-atomic chains. Finally, we conclude our results.

2 Theoretical Methods: Non-collinear Density Functional Theory and PAW methods

We have calculated magnetism of Ni_n ($n=1-5$) chains supported on the Au(110)-(1 \times 2) surface based on Density Functional Theory [34, 35] and the Methods of Projection of Augmentation Wave (PAW) [36] with the plane-wave base set and GGA Perdew-Burke-Ernzerhof’s exchange-correlation potential [37]. The PAW methods used in VASP program [38–40] is as accurate as frozen-core all-electron methods and hopefully improved to include all-electron relaxation. Our calculations include the non-collinear effects and the spin-orbit coupling which is proved important to heavy metals such as gold. In non-collinear formula, a magnetic moment as a vector can point to any direction in space. The orbital polarization (OP) interaction isn’t included in our calculations.

The basic theory used in this paper is Hobbs’s fully unconstrained non-collinear DFT formulas based on plane wave basis sets and all-electron PAW methods [40, 41]. Instead of distributing local quantization axes for every atoms, which is used in programs based on atom sphere approximation (ASA) or others analogous methods [42], Hobbs’s theory adopts only one global quantization axis and the vectors of magnetic electronic density are varying smoothly and continuously, which is more suited for the calculations of itinerant magnetism in transition metal materials.

In non-collinear density functional theory [40–42], the total energy is the functional of a density matrix $n_{\alpha\beta}$ where α and β are the spin index along a defined quantization axis. $\alpha = \uparrow$ or \downarrow represent the spin angular momentum point to the positive direction or negative direction of the quantization axis. The sum of the diagonal elements is the total charge density, that is $n_{Tr} = \sum_{\alpha} n_{\alpha\alpha}$. In a non-collinear magnetic system, the off-diagonal elements are non-zero. The 2 \times 2 matrix can be expanded using the complex matrix basis ($I, \sigma_x, \sigma_y, \sigma_z$) and expressed as

$$n_{\alpha\beta} = [n_{Tr}\delta_{\alpha\beta} + \vec{m} \cdot \vec{\sigma}_{\alpha\beta}]/2, \quad (1)$$

where $\vec{m} = \sum_{\alpha\beta} n_{\beta\alpha} \cdot \vec{\sigma}_{\alpha\beta}$ is the magnetic electronic density and $\vec{\sigma}$ is the Pauli matrix. In PAW methods, the pseudo-density matrix can be expressed using the pseudo-wave functions as

$$\tilde{n}_{\alpha\beta}(\vec{r}) = \sum_n f_n \langle \tilde{\Psi}_n^\beta | \vec{r} \rangle \langle \vec{r} | \tilde{\Psi}_n^\alpha \rangle, \quad (2)$$

where f_n is the occupation number. The total electronic density matrix $n_{\alpha\beta} = \tilde{n}_{\alpha\beta} + n_{\alpha\beta}^1 - \tilde{n}_{\alpha\beta}^1$, where $n_{\alpha\beta}^1$ and $\tilde{n}_{\alpha\beta}^1$ are the on-site electronic density matrixes. The total energy as the sum of three parts $E = \tilde{E} + E^1 - \tilde{E}^1$, where \tilde{E} the smooth functional of the pseudo-density matrix $\tilde{n}_{\alpha\beta}(\vec{r})$ is evaluated on a regular grid, E^1 and \tilde{E}^1 the functionals of on-site electronic density matrixes $n_{\alpha\beta}^1$ and $\tilde{n}_{\alpha\beta}^1$ are calculated on radical support grid around every atom.

The Kohn-Sham Hamilton and Kohn-Sham equation can be obtained from the variation of total energy to the soft pseudo-density matrix and written as

$$\begin{aligned} H^{\alpha\beta}[n] = & -\frac{1}{2}\Delta\delta^{\alpha\beta} + \tilde{v}_{eff}^{\alpha\beta} \\ & + \sum_{(ij)} |\tilde{p}_i\rangle (\hat{D}_{ij}^{\alpha\beta} + {}^1D_{ij}^{\alpha\beta} - {}^1\tilde{D}_{ij}^{\alpha\beta}) \langle \tilde{p}_j|, \\ \sum_{\beta} H^{\alpha\beta} |\tilde{\Psi}_n^\beta\rangle = & \varepsilon_n S^{\alpha\alpha} |\tilde{\Psi}_n^\alpha\rangle. \end{aligned} \quad (3)$$

where $S^{\alpha\alpha}$ is the overlapping operator, $\tilde{D}_{ij}^{\alpha\beta}$, ${}^1\hat{D}_{ij}^{\alpha\beta}$ and ${}^1D_{ij}^{\alpha\beta}$ are the non-local interaction obtained by the PAW transformation, which are equivalent to the nonlocal pseudo-potential in the ultrasoft-potential methods. In non-collinear DFT formulas, the one-electron effective potential $\tilde{v}_{eff}^{\alpha\beta} = v_H(r)\delta_{\alpha\beta} + v_{xc}(r)\delta_{\alpha\beta} + \vec{b}(r) \cdot \vec{\sigma}^{\alpha\beta}$, which is the summation of electrostatic potential $v_H(r)$, the nonmagnetic part of GGA exchange-correlation correction $v_{xc}(r)$ and the magnetic exchange-correlation potential $\vec{b}(r) \cdot \vec{\sigma}^{\alpha\beta}$, where $\vec{b} = \delta E_{xc} / \delta \vec{m}(r)$. The magnetic exchange-correlation potential will potentially enhance magnetic moments in non-collinear calculations.

The spin-orbit coupling enters into PAW formulas by all-electron part of PAW Hamiltonian and is expressed as

$$H_{SOI}^{\alpha\beta} = \frac{\hbar^2}{(2m_e c)^2} \sum_{ij} \langle \phi_i | \frac{1}{r} \frac{dV_{sphere}}{dr} | \phi_j \rangle |\tilde{p}_i\rangle \vec{\sigma}_{\alpha\beta} \cdot \vec{L}_{ij} \langle \tilde{p}_j|. \quad (4)$$

where \tilde{p}_i is the projector function and ϕ_i all-electron wave function. The one-electron effective potential is modified $\tilde{v}_{eff}^{\alpha\beta} \rightarrow \tilde{v}_{eff}^{\alpha\beta} + \tilde{H}_{SOI}^{\alpha\beta}$, and the same time, one part of nonlocal PAW potentials is modified according to $\hat{D}_{ij}^{\alpha\beta} \rightarrow \hat{D}_{ij}^{\alpha\beta} = \sum_L \int (\tilde{v}_{eff}^{\alpha\beta}(r) + \tilde{H}_{SOI}^{\alpha\beta}(r)) \hat{Q}_{ij}^L(r) dr$. The roles of spin-orbit interaction in ${}^1\hat{D}_{ij}^{\alpha\beta}$ and ${}^1D_{ij}^{\alpha\beta}$ are similar to $\hat{D}_{ij}^{\alpha\beta}$, however they are calculated only within atom sphere. In the calculations of real material, they adopt the values in the calculations of isolate atom and don't update in Kohn-Sham self-consistent

loop. More information on non-collinear density functional theory within PAW methods can be found in the reference [40].

The atoms can have their initial magnetic moments by constructing the magnetic electronic density and the magnetic moments around each of atoms are equal to their desired values. If the initial total magnetic moments point \vec{n} direction, generally the direction of total moment changes in Kohn-Sham self-consistent loop. We can use the constrained DFT calculations to fix the direction of magnetic moments. Our self-consistent calculations show that the directions of magnetic moments change very small in ferromagnetic materials although using the unconstrained DFT calculations (see the table.(2) in section 4.1). In real ferromagnetic materials, the directions of magnetic moments are hard to change, once the magnetic domains have formed. This is because the change of magnetization direction must include the changes of magnetic moments of all magnetic atoms in the materials. An external magnetic field can force to change the direction of magnetic moments. Of course there exists an easy magnetization axis which is stable direction of magnetic moments. We need the 'strongest' magnetic field to change direction of magnetic moments away from the direction of the easy magnetization axis. However for the materials with more complex magnetic structure such as the canted and spiral magnetic structures, the relaxations of directions of magnetic moments are intrinsic, the use of unconstrained DFT is essentially important [40, 41].

3 The magnetism of 3d transition metal atoms absorbed on Au(110)-(1×2) and Au(111) surface

The missing row Au(110) surface reconstructs from Au(110) surface by having missed closed-packed Au chains every others, and forms one-dimensional trough along the close-packed A- $[\bar{1}10]$ direction. We construct a crystal slab with 4 atomic layers including 28 gold atoms. At the first step we optimized the lattice constant of gold crystal which is about 4.2Å. In the procession of optimization, the RMM-DIIS algorithm [38] is applied to the total-energy minimum with plane-wave energy cutoff 229.9eV and the 6x6x6 Monkhorst-Pack K points mesh. Now the size of super-cell is 11.8Å×8.4Å×5.94Å.

We add a vacuum layer by extending the super-cell along C- $[110]$ direction. The size along C- $[110]$ direction of super-cell including vacuum layer is equal to 16Å. The lattice constant of surface is generally smaller than that of the crystal. Thus we optimized the slab with vacuum layer together. Based on the optimized lattice constant, the size of the super-cell is 11.523Å×8.148Å×15.52Å. The vacuum layer is about twice thicker than thickness of the slab. For the optimized Au(111) surface, the size of super-cell is about 11.5Å×9.97Å×20Å including 64 gold atoms. In above optimizations, we only change the lattice

constant. The initial structures are constructed by placing the 3d transition metal atoms on the hollow sites of the Au(111) and Au(110)-(1×2) surface in the trough (Fig. 1). The initial structures are optimized for all atoms except for the bottom atoms by having used the conjugate-gradient Methods. The K-points meshes of 2×2×1 or Γ point are used to sampling the first Brillouin-zone in the corresponding calculations of the electronic structure for Au(110)-(1×2) and Au(111) surfaces respectively. In this work we use smaller k-points mesh to more efficiently optimize surface structures.

We use both collinear and non-collinear density functional calculations but mainly present the non-collinear results. In non-collinear DFT calculation, we use the optimized structures from collinear DFT calculation. Based on the relaxed structures, we calculate more exactly the electronic structures using the RMM-DIIS algorithm [38] with the (6×6×1) Monkhorst-Pack grids sampling the first Brillouin zone. If the changes of the total energies are smaller than 0.0001eV between two electronic self-consistent (SC) steps the SC-loops break. We set the Methfessel-Paxton smearing width equal to 0.20eV to accelerate the speed of convergence. The energy-cutoffs of plane-wave for different atoms are summarized in table (1). The magnetic moments for a single atom are calculated by considering the electrons in a Wigner-Seitz sphere centered at the position of the atom. The Wigner Seitz Radii for 3d transition metal atoms are also summarized in table (1). We choose the C-[110] direction as the quantization axis. We emphasize the influence of surface deformation on the orbital moments of the absorbed atoms. The orbital polarization interaction omits in this work but includes the spin-orbit coupling interaction. We obtain smaller orbital moments compared with pervious density functional calculation including the orbital polarization interaction [44].

3.1 *The influence of structural relaxations on the magnetism of a single absorbed 3d transition atom*

It's seem that collinear DFT calculation is enough to the study of magnetism of a single transition metal absorbed on the gold surface. However, if we want to know the direction of magnetic moments relative to the surface, we must use the non-collinear DFT formulas. These results for single absorbed atom will be compared with the results of one-dimensional atomic chains. At first step, we calculate the magnetic moments of the absorbed 3d atoms on the Au(110)-(1×2) and Au(111) surfaces including the spin-orbit coupling interactions and non-collinear calculations. From Fig. 2, we can see that the spin moments reach the maximum in the middle of the group. The large spin moment of the absorbed Mn atom is about $4.163\mu_B$ on the Au(110)-(1×2) surface. We can see from the left panel of the figure that the spin moment of the absorbed Cr atom is the second largest when including the spin-orbit coupling interactions

and non-collinear calculations. The change of magnetic moments per absorbed magnetic atom across the 3d row has been found in many other *ab initio* calculations such as 3d atoms on Au(001), Ag(001) [45] and Cu(001) [46] surfaces. Our results are consistent very well with these results although the energy cutoffs of plane-waves are not too large in our calculations.

Both the electronic correlations and the crystal field have significant influence on the orbital moments of the absorbed 3d atoms. If the electronic correlation is stronger than the crystal fields, the orbital moment is large, otherwise small. The absorbed Ti, V, Co atoms have visible orbital moments $0.086\mu_B$, $0.082\mu_B$ and $0.092\mu_B$ on the Au(110)-(1 \times 2) surface, and $0.006\mu_B$, $0.071\mu_B$ and $0.247\mu_B$ on the Au(111) surface respectively. Cabria, et.al obtained larger orbital moment (about $0.5\mu_B$) of Fe and Co atoms absorbed on Au(001) surface using the spin polarization relativistic KKR methods including the orbital polarization term [44, 45]. The usual exchange-correlation potentials (LDA or GGA) underestimate the electronic correlations such as the Coulomb correlation and the orbital polarization, thus the obtained orbital moments in this work are generally small compared with experimental values [20–22, 44] although our work includes the spin-orbit coupling interaction. The small values of orbital moments of the absorbed Cr atoms in our calculations are not related to the crystal field but to its electronic structure. In the individual Cr atom, five 3d-electrons half-fill the 3d states, the total orbital moment is very small.

The coordination number of surface atoms is generally smaller than those in bulk. So the magnetism of surface is generally stronger than that in bulk. The supported atoms on the surface are in the environment similar to the surface atoms. Based on the same logic, the supported atoms on the surface have possibly strong magnetism. The lack of the orbital polarization isn't the obstacle to study the structural influence on the orbital moments. In order to clearly illustrate the effects of the crystal deformations (or the cubic distortions), we compare the results on the deformed surface with that on the perfect Au(110)-(1 \times 2) surface. The absorbed 3d atoms on the perfect surface still modify their positions to reach their stable positions, while the surface atoms are fixed. We find from Fig. 3 that the surface relaxations generally quench the orbital moments of the absorbed 3d atoms except for the absorbed V and Ti atoms. The changes of the orbital moments in response to the relaxations are closely related to the changes of the depth of the 3d atoms embedded in the trough of the reconstructed Au(110) surface. The absorbed atoms are deeper in the trough, their orbital moments are quenched to smaller values due to the stronger crystal field. The absorbed V atom rises above the top row of the trough after the relaxations and its orbital moment enhances, opposes to the orbital quenching for the other 3d atoms except for the absorbed Ti atom. This is due to the weaker crystal field above the surface than that in the trough. The absorbed Ti atom has almost the same height as the top row after the relaxations and its orbital moment slightly increases. Thus our results indicate

that the surface relaxation decreases the orbital moments of the absorbed 3d atoms with the excess half-filled 3d states and increases the orbital moments of the absorbed atoms with less half-filled 3d states on Au(110)-(1×2) surface.

The 3d density of states of the absorbed 3d atoms on the two surfaces are shown in Fig. 5. The absorbed Ti, V, Co atoms on the Au(110)-(1×2) surface and V, Co atoms on the Au(111) surface have large 3d densities of states at the Fermi energies and large orbital moments too. We get the same arguments on the magnetism of Ni_n ($n=1-5$) chains. Large density of state $N(E_f)$ at Fermi energy is advantaged to the formation of the orbital moments. The single Ni atom has small magnetic moment, however we can see in section 4 the Ni clusters such as one-dimensional Ni chains have significant magnetic moments on the Au surface. The exchange interactions between Ni atoms prevent from the decay of magnetic moments of Ni atoms.

4 The magnetism of Ni atomic chains

The initial Ni chains are located in the trough along the A-[1 $\bar{1}$ 0] direction with nearest-neighbor distance about 2.88Å the same as the nearest-neighbor distance of the missed Au chain [Fig. 1]. The surface slab includes 4 atomic layers with 56 Au atoms and the size of the super-cell is 23.046Å×8.148Å×15.52Å. We have relaxed the initial structures using the conjugate-gradient Methods. The 2×2×1 K-points mesh is used to sampling Brillouin-zone in the corresponding electronic-structure calculations. Based on the relaxed structures, we calculated their electronic structures more exactly using RMM-DIIS algorithm with the (4×4×1) Monkhorst-Pack grids sampling the first Brillouin zone. The other information is the same as in the calculations for single 3d atoms.

We have also calculated the magnetism of free-standing Ni chains by removing all surface atoms but still preserving in the same box cell. There are mirror atomic chains because of periodic boundary condition along three directions. The interaction of free-standing chains with its mirror atomic chains are small and negligible if the box cell is large enough. We have only chosen short chains Ni_n where n less than 6 and large box size 23Å along the direction parallel the chain so that the ends of chains are far away from the boundaries of the box cell. The energetically favorable configuration of one-dimensional free-standing chains has zigzag shapes and not straight line. The Ni_n atomic chains in the trough of Au(110)-(1×2) surface are straight. As we optimize the structures of free-standing chains, all atoms are only allowed modified their position along the direction of chains and the optimized free-standing Ni chains still keep a straight line shape. We try to compare the results of surface-support straight chains with those of free-standing straight chains. The quantization axis is

still along the C-[110] direction in this section.

4.1 Magnetism of Ni_n ($n=1-5$)

All Ni atoms in the cell have their initial magnetic moments in our calculations. We calculate the total energies, the spin and orbital magnetic moments of the supported Ni chains when they are magnetized along A-[$\bar{1}\bar{1}0$] direction parallel to the chains or C-[110] direction perpendicular to the chains respectively. The magnetization of an atomic chain in this paper means that the magnetic moments for every Ni atom align along the same direction. The values of initial moments of Ni atoms are all the same, however the values after the self-consistent calculations are probably not the same for all Ni atoms. The orientations of magnetic moment may manually change to simulate the different magnetizing directions. In a single self-consistent calculation, the directions of magnetic moments change very small for the ferromagnetic Ni chains although we have used the unconstrained Density Functional calculations (see the table.(2)).

The chains become short after the relaxations and the average nearest-neighbor distance of Ni_5 chain is about 2.75 Å shorter than 2.88 Å that of initial structure [the insert figure of Fig.5(b) and Fig.1]. We choose two magnetizing directions: A-[$\bar{1}\bar{1}0$] direction parallel to the chain and C-[110] direction perpendicular to the chain. The size-dependence magnetic moments are shown in Fig. 5 (a). From this figure we can see that the spin moments of a single adsorbed Ni atom are small, $0.147\mu_B$ for the magnetization along C-[110] direction and $0.127\mu_B$ for A-[$\bar{1}\bar{1}0$] direction. The spin moments per atom of the Ni_2 chain increase to $0.455\mu_B$ for A-[$\bar{1}\bar{1}0$] direction and $0.464\mu_B$ for C-[110] directions. The spin moments of Ni_3 have slightly decrease for C-[110] direction but large decrease for A-[$\bar{1}\bar{1}0$] direction. The spin moments decrease slightly and try to keep a constant as the chain length increases above 4. Our results show that the spin moments of Ni atoms on the reconstructed Au(110) surface are smaller than the value $0.675\mu_B$ in crystal Ni having been calculated using the same methods in our work.

The magnetic order is an important aspect of material magnetism. Experimentally the long ferromagnetic order is found for Co chains stabilized above a finite temperature on Pt(997) surface [5]. Above the temperature, the long ferromagnetic order is destroyed and changed into the short ferromagnetic fragments. In our calculations, the short Ni chains are ferromagnetic. The Fig.6 shows the ferromagnetic order of the surface supported Ni_5 chains for the magnetization for C-[110] and A-[$\bar{1}\bar{1}0$] directions. The spin-polarizations of surface Gold atoms near the Ni chain are induced by the magnetic Ni atoms, which almost disappear for Gold atoms far from the Ni chain. We have also calcu-

lated the anti-ferromagnetic configurations, non-magnetic configurations and other non-collinear magnetic configurations and found their energies higher than that of the ferromagnetic configuration. Thus our calculations show that the Ni chains with ferromagnetic order are most energetically favorable. It is interesting to find from this figure that, when magnetizing the Ni chains parallel to the chain, the orbital moments are larger than that perpendicular to the chains. The spin moments for every Ni atom of the ferromagnetic Ni chain almost don't change their directions after the Kohn-Sham self-consistent calculations for all three magnetization directions [table. (2)]. The spin moment of the middle atom is smaller than that of other atoms and thus the short Ni chain isn't in perfect ferromagnetic order. The larger spin-moments for atoms at two ends are because of the smaller coordination number compared with the middle atoms.

The interaction between supported Ni_n chain and surface can be measured with the interaction energy $E_I = E^{tot} - E^s - E^f$ where E^{tot} is the total energy, E^s the energy of slab with relaxed surface and E^f the energy of free-standing chain. We generally calculate the interaction energy per atom, which removes the effects of simple summation. The interaction energies are generally negative. Fig. 5(b) shows that the interaction energies of the Ni chains with the surface increase with the chain lengths. In our classical molecular dynamics simulation, we have found the oscillation of interaction energy for longer chains induced by lattice misfit [28]. These results indicate that short Ni chains are more energetically favorable on Au(110)-(1×2) surface. This is consistent with the experiments [27] in which most of Ni chains are shorter than 6. Additionally, we calculate the density of states of the Ni_n ($n=1-5$) chains. From the Fig. 7, we can see that the densities of states of 3d states of Ni_5 chain changes very small when the magnetization changes from C-[110] direction to A-[$\bar{1}\bar{1}0$] direction and the spin magnetic moment does also change very small [Fig. 7]. From the figure 5, the changes of orbital moments are more significant if the magnetizing directions change. Although the orbital moments are underestimated due to the absence of (OP) orbital polarization term, our results still show that magnetic anisotropy are closely related to the orbital degree of freedom. For compact magnetic islands on metal surface such as Co/Pt(111) [47], the orbital moments decrease with increasing island sizes. This is because only atoms at the edge of island have significant contributions to the total orbital moments. However, for one-dimensional island all atoms have significant contribution to the total orbital moments. The orbital moments per atom keep constant as the lengths of chains beyond 4.

4.2 The magnetic anisotropy of Ni_5 chain

In the above subsection we have chosen two magnetization directions A-[$\bar{1}10$] and C-[110]. In this subsection, we study the magnetic anisotropy of the Ni_5 chain and show that C-[110] direction is along the easy magnetization axis. The magnetic anisotropy energies in S_1 and S_2 planes are defined as $\delta E_1 = E^C - E^A$ and $\delta E_2 = E^C - E^B$ respectively. E^A , E^B and E^C are the total energies when magnetizing the chain along A-[$\bar{1}10$] ($\theta = 0^\circ$), B-[001] ($\phi = 0^\circ$) and C-[110] ($\theta = 90^\circ$) directions [53]. The magnetic anisotropy of one-dimensional structure is more prominent than compact structures such as surface and bulk. Fig.8 shows the total energies, the spin and orbital moments change with two magnetization angles in above two planes. We find from Fig. 8(a,b) that there are weak magnetic anisotropy in S_1 plane and relative strong the magnetic anisotropy in S_2 plane. The magnetic anisotropy energies are 0.158(meV/atom) and 0.524(meV/atom) respectively in the two planes. The shape anisotropy determines the large difference of magnetic anisotropy energy in two plane because of one-dimension characteristic of mono-atomic chain. In the same plane such as the plane S_1 , the magnetic anisotropy is determined by spin-orbit coupling. The easy magnetization directions in both S_1 and S_2 planes are all along C-[110] direction ($\theta = 90^\circ$ and $\phi = 0^\circ$), which is perpendicular to the chain and the surface. The magnetic anisotropy energies can be represented as $K_0 + K_1 \sin^2(\theta)$ in S_1 plane and $K'_0 + K'_1 \sin^2(\phi)$ in S_2 plane [26, 52]. The parameters $K_0=0.158$ (meV), $K_1=-0.158$ (meV) in S_1 and $K'_0=0.0$ (meV), $K'_1=0.62$ (meV) in S_2 are obtained by fitting the magnetic anisotropy curves using above two functions. The magnetic anisotropy isn't good fit with $K_0 + K_1 \sin^2(\theta)$ in S_1 . The underlying reasons are (1) there isn't simple cubic symmetry in the region where the one-dimensional atomic chain absorbed; (2) the heterogeneously distributed the nearest nearby distances along the chain induced by the lattice misfit between the chain and the substrate. On the other hand, the value of K_1 is close to the lowest limit of allowed error in total energy about ± 0.1 meV, thus more accurate calculations are required. Our results also show that K_1 (or K'_1) isn't equal to the simple $\delta E_1 = E^C - E^A$ (or $\delta E_2 = E^C - E^B$).

Experimentally, the values of magnetic anisotropy energy are from 1 meV to 10 meV for magnetic clusters on metal surface and from 0.1 mV to 1.0 meV for magnetic film. Based on our calculations, the magnetic anisotropy energies for Ni chains on the reconstructed Au(110) surface are close to the values of magnetic film. This is because the atoms on Ni chain replace the atoms of first layer of original surface and have almost the same coordinate number in their monolayer film. The experiment in Co/Pt(997) has shown that the anisotropy energy about 2 meV for the monatomic Co chains and 0.14 meV for the monolayer Co film on Pt(997) surface [5]. From Fig. 8(e) we can find that the orbital moments reach the minimum when magnetizing

the Ni chain along the easy magnetization direction. Fig. 8(f) also shows that the orbital moments almost keep a constant when the magnetization angle ϕ changes in S_2 plane. The directions of orbital moments for every Ni atoms on the chain are almost parallel to their spin moments when the magnetizations are along A- $[\bar{1}\bar{1}0]$ and C- $[110]$ axes, or anti-parallel to their spin moments for the magnetization along B- $[001]$ axis. From the curve of magnetic anisotropy energy in S_2 plane in Fig. 8(b) it's most energetically unfavorable when the spin moment of the Ni chain points to B- $[001]$ direction ($\phi = 90^\circ$).

4.3 *The magnetic anisotropy of free-standing Ni_5 chain and Discussion*

In order to illustrate the surface influence on the magnetic anisotropy, as a comparison, we also calculate the magnetic anisotropy of free-standing Ni_5 chain in the same box. All calculating details are the same as those of the surface-supported Ni_5 chain except for removing the surface atoms. The average nearest-neighbor distance is about 2.196 Å shorter than 2.77 Å for the surface-support Ni_5 chain and 2.5 Å in Ni crystal. The changes of densities of states of 3d states for free-standing Ni chain are that the majority-spin-up densities of states are far from to the Fermi Energy. The larger densities of states at Fermi energy contributed by the minority-spin-down DOS indicate that there are larger spin and orbital moment magnetic moments for free-standing Ni chain.

We only consider the changes of the total energies with the angle θ . From the Fig. 8 (g) we can see that the easy magnetization direction is now parallel to the chain which is different from perpendicular to the chain for the surface-supported Ni_5 chain. For free-standing chain we find $K_0=0.0$ (meV) and $K_1=8.4$ (meV) in S_1 . The anisotropy energy is large compared with the surface-supported Ni_5 chain. The change of the sign of K_1 compared with surface-supported chain means that the easy magnetization axis change in S_1 plane. The change of the easy magnetization axis had been found in other theoretical works such as Co chains on Pd(110) surface [18]. Experimentally, the changes of easy magnetization axis are found in the growth of magnetic film on metal surface when the thickness of film is beyond a critical value d_c . The transitions from in-plane to perpendicular plane for Ni/Cu(100) [48] and inversely from perpendicular to in-plane for Fe/Ag(100) [49] and Co/Au(111) [50] are found at critical coverage about 5-7 ML. The transitions are close related with the transitions from films with heterogeneously distributed strains to films with homogeneously distributed strains once beyond critical thickness. The atomic chains in this work are found in initial stage of film growth and have the easy magnetization axis perpendicular to the surface. Whether the easy magnetization axis changes after a monolayer had completely grown on the surface is interesting topic in our following work.

The spin moments keep almost constant when the magnetization angle changes from $\theta = 0^\circ$ to $\theta = 90^\circ$. The spin moment about $1.14\mu_B$ per atom is significantly large than its values in Ni crystal $0.675\mu_B$. The behavior of the orbital moment is similar to the surface-supported Ni_5 chain, that is, reaches the minimum when perpendicularly magnetizing the chain. The underlying reason is geometric, that is, the orbital currents (or Molecular Currents) of neighbor atoms have large overlapping and their cancelations are also large which is disadvantageous to form larger orbital moments. The values of orbital moments from $0.2\mu_B$ to $0.6\mu_B$ are larger one power of the values of surface supported Ni atoms. The easy magnetization axis of free-standing Ni chain A- $[\bar{1}\bar{1}0]$ is different from the easy magnetization axis of surface-supported chain C- $[110]$. The orbital moment reaches its maximum along the easy magnetization axis A- $[\bar{1}\bar{1}0]$, $\theta = 0^\circ$ for free standing chain, which is consistent with the results for magnetic monolayer, [22, 51] but reaches the minimum along the easy magnetization C- $[110]$ axis $\theta = 90^\circ$ for the surface-supported chain. Thus our results show that the surface effects change the easy magnetization axis and decrease both the magnetic anisotropy energy and the magnetic moment of free standing chains because of the increase of coordination number for every atom on a surface.

5 Conclusion

Based on the Density Functional Theory, we have calculated the magnetic anisotropy of the supported Ni chains and free-standing chain. The easy magnetization axis of the supported Ni chain is perpendicular to the chain and surface but parallel to the chain for free standing chain. The different easy magnetization axis for the supported and free standing chain is also found in density functional calculations of other system. Our results indicate the closed relationship between the magnetic anisotropy and orbital moments of the Ni chains. In the environments of crystal, the orbital moment is generally quenched to small value due to the splitting of crystal field. Compared with spin moment, orbital moment is more sensitive to the change of magnetization direction. The orbital quenching changes with the change of magnetized directions. The magnetic anisotropy of materials are determined both by the orbital quenching and spin-orbit coupling. For a single absorbed atom, the surface relaxations generally deform the surface and modify the positions of the absorbed atoms. If the relaxations lift the absorbed atom out of the trough on the constructed Au(110) surface, the orbital moments enhance due to weaker crystal fields and if the relaxations make the absorbed atoms deeper embedded in the trough the orbital moments quench to smaller values due to the stronger crystal fields.

Acknowledgement

The one of authors (W. Fan) is greatly indebted to Prof. Q. Q. Zheng, Dr. J. L. Wang, Prof. L. J. Zou and Prof. Z. Zeng for their helpful discussions. This work run on computers in Center for computational science, Hefei Institutes of Physical Science and on LSSC in Institute of Computational Mathematics and Scientific/Engineering Computing, Chinese Academy of Sciences. X. G. Gong is additionally supported by the National Science Foundation of China, the special funds for major state basic research and CAS projects and Knowledge Innovation Program of Chinese Academy of Sciences under KJCX2-SW-W11.

References

- [1] H. J. Elmers, J. Hauschild, H. Höche, U. Gradmann, H. Bethge, D. Heuer, and U. Köhler, Phys. Rev. Lett. **73** (1994) 898.
- [2] J. Shen, R. Skomski, M. Klaua, H. Jenniches, S. S. Manoharan, and J. Kirschner, Phys. Rev. B **56** (1997) 2340.
- [3] J. Hauschild, H. J. Elmers, U. Gradmann, Phys. Rev. B **57** (1998) R677.
- [4] M. Pratzer, H. J. Elmers, M. Bode, O. Pietzsch, A. Kubetzka, and R. Wiesendanger, Phys. Rev. Lett. **87** (2001) 127201.
- [5] P. Gambardella, A. Dallmeyer, K. Maiti, M. C. Malagoli, W. Eberdardt, K. Kern, and C. Carbone, Nature (London) **416** (2002) 301.
- [6] P. Gambardella, M. B. lanc, L. Bürgi, K. Kuhnke, and K. Kern, Surf. Sci. **449** (2000) 93.
- [7] P. Gambardella, M. Blanc, K. Kuhnke, and K. Kern, Phys. Rev. B **61** (2000) 2254.
- [8] Dongqi Li, Chengtao Yu, J. Pearson, and S. D. Bader, Phys. Rev. B **66** (2002) 020404.
- [9] C. Boeglin, S. Stanescu, J. P. Deville, P. Ohresser, and N. B. Brookes, Phys. Rev. B **66** (2002) 014439.
- [10] H. Dreyssé, C. Demangeat, Surf. Sci. Rep. **28** (1997) 65.
- [11] V. Bellini, N. Papanikolaou, R. Zeller, and P. H. Dederichs, Phys. Rev. B **64** (2001) 094403.
- [12] K. Wildberger, V. S. Stepanyuk, P. Lang, R. Zeller, and P. H. Dederichs, Phys. Rev. Lett. **75** (1995) 509.
- [13] B. Lazarovits, L. Szunyogh, P. Weinberger, B. Ujfalussy, Phys. Rev. B **68** (2003) 024433.

- [14] M. Eisenbach, B. L. Györfy, G. M. Stocks, and B. Újfalussy, Phys. Rev. B **65** (2002) 144424.
- [15] M. Komelj, C. Ederer, J. W. Davenport, and M. Fähnle, Phys. Rev. B **66** (2002) 140407.
- [16] D. Spišák and J. Hafner, Phys. Rev. B **65** (2002) 235405.
- [17] D. Spišák and J. Hafner, Phys. Rev. B **67** (2003) 214416.
- [18] J. Dorantes-Dávila and G. M. Pastor, Phys. Rev. Lett, **81** (1998) 208.
- [19] R. Druzinic and W. Hübner, Phys. Rev. B **55** (1997) 347.
- [20] M. S. S. Brooks, P. J. Kelly, Phys. Rev. Lett. **51** (1983) 1708 .
- [21] O. Eriksson, M. S. S. Brooks, B. Johansson, Phys. Rev. B **41** (1990) 7311.
- [22] I. V. Solovyev, A. I. Liechtenstein, K. Terakura, Phys. Rev. Lett. **80** (1998) 5758.
- [23] O. Hjortstarm, K. Baberschke, J. M. Wills, B. Johansson, and O. Eriksson, Phys. Rev. B **55** (1997) 15026.
- [24] I. V. Solovyev, Phys. Rev. Lett. **95** (2005) 267205. (or arXiv:cond-mat/0510100)
- [25] F. Fuchs, J. Furthmüller, F. Bechstedt, M. Shishkin, and G. Kresse, Preprint-arXiv:cond-mat/0604447, 2006
- [26] Harvey Brooks, Phys. Rev. **58** (1940) 909.
- [27] A. Hitzke, M. B. Hugenschmidt, R. J. Behm, Surface Science, **389** (1997) 8.
- [28] W. Fan, X. G. Gong, and W. M. Lau, Phys. Rev. B **66** (2002) 115418.
- [29] K. D. Gross, D. Riegel, and R. Zeller, Phys. Rev. Lett. **63** (1989) 1176.
- [30] K. D. Gross, D. Riegel, and R. Zeller, Phys. Rev. Lett. **65** (1990) 3044.
- [31] M. C. Hanf, C. Pirri, J. C. Peruchetti, D. Bolmont, and G. Gewinner, Phys. Rev. B **36** (1987) 4487.
- [32] D. Riegel, L. Büermann, K. D. Gross, M. Luszik-Bhadra, and S. N. Mishra, Phys. Rev. Lett. **62** (1989) 316.
- [33] J. E. Ortega and F. J. Himpsel Phys. Rev. B **47** (1993) 16441.
- [34] P. Hohenberg and W. Kohn, Phys. Rev. **136** (1964) B864.
- [35] W. Kohn and L. J. Sham, Phys. Rev. **140** (1965) A1133.
- [36] P. E. Blöchl, Phys. Rev. B **50** (1994) 17953.
- [37] J. P. Perdew, K. Burke, and M. Ernzerhof, Phys. Rev. Lett. **77** (1996) 3865.
- [38] G. Kresse and J. Furthmüller, Comput. Mater. Sci. **6** (1996) 15.

- [39] G. Kresse and D. Joubert, Phys. Rev. B **59** (1999) 1758.
- [40] D. Hobbs, G. Kesse, J. Hafner, Phys. Rev. B **62** (2000) 11556; M. Marsman, *Magnetism*, the talks and hands-on sessions of VASP Workshop, Vienna (2003).
- [41] D. Hobbs, J. Hafner, D. Spišák Phys. Rev. B **68** (2003) 014407.
- [42] L. M. Sandratskii, Advances in Physics, **47** (1998) 91.
- [43] The energy cutoffs for plane wave adopt the values distributed by VASP code (CMS group at University of Vienna).
- [44] B. Nonas, I. Cabria, R. Zeller, and P. H. Dederichs, T. Huhne and H. Ebert, Phys. Rev. Lett. **86** (2001) 2146.
- [45] I. Cabria, B. Noas, R. Zeller, and P. H. Dederichs, Phys. Rev. B **65** (2002) 054414.
- [46] V. S. Stepanyuk, A. N. Baranov, W. Hergert, and P. Bruno, Phys. Rev. B **68** (2003) 205422.
- [47] P. Gambardella, S. Ruspoi, T. Cren, N. Weiss, H. Brune, C. R. Physique, **6** (2005) 75.
- [48] B. Schulz and K. Baberschke, Phys. Rev. B **50** (1994) 13467.
- [49] Z. Q. Niu, J. Pearson, and S. D. Bader, Phys. Rev. Lett **70** (1993) 1006.
- [50] R. Allenspach, M. Stampanoni, and A. Bischof, Phys. Rev. Lett **65** (1990) 3344.
- [51] Patrick Bruno, Phys. Rev. B **39** (1989) 865.
- [52] Gabriel Autès, Cyrille Barreteau, Daniel Spanjaard, and Marie-Catherine Desjonquères, Preprint:arXiv:cond-mat/0603121, (2006).
- [53] The magnetic anisotropy energy (MAE) also be measured using the difference of the sums of Kohn-Sham eigenvalues which have been used in LMTO and LAPW program with (ASA) Atom sphere Approximation for monatomic systems. T. Burkert, O. Eriksson, P. James, S.I. Simak, B. Johansson, and L. Nordström, Phys. Rev. B **69** (1985) 104426. M. Weinert, R.E. Watson, and J.W. Davenport, Phys. Rev B **32** (1985) 2115. G. H. O. Daalderop, P. J. Kelly, and M. F. H. Schuurmans, Phys. Rev. B **41** (1990) 11919.

Table 1

The Wigner Seitz Radius-WSR (\AA) and Energy-Cutoff of plane wave-Ecut (eV) for PAW potentials of 3d transition metal T_{3d} =V, Ti, Cr, Mn, Fe, Co, Ni, Cu. [43] The real energy cutoff for T_{3d}/Au is $\text{Ecut}(T_{3d}/\text{Au}) = \text{Max} [\text{Ecut}(T_{3d}), \text{Ecut}(\text{Au})]$.

	Ti	V	Cr	Mn	Fe	Co	Ni	Cu	Au
WSR	1.323	1.323	1.323	1.323	1.302	1.302	1.286	1.312	1.503
Ecut	178.4	192.6	227.1	269.9	267.9	268.0	269.6	273.2	229.9

Table 2

The spin and orbital magnetic moments (Bohr) for every atoms of Ni_5 chain when the magnetization directions are along A-[$\bar{1}\bar{1}0$], B-[001] and C-[110] respectively. This table shows that the directions of spin magnetic moments are almost unchanged in Kohn-Sham self-consistent loop although we have used the unconstrained DFT calculations.

	A-[$\bar{1}\bar{1}0$]			B-[001]			C-[110]		
	M_A	M_B	M_C	M_A	M_B	M_C	M_A	M_B	M_C
Ni ₁	0.434	0.0	-0.006	0.0	0.411	0.0	0.017	0.0	0.430
Ni ₂	0.449	0.0	0.006	0.0	0.426	0.0	-0.012	0.0	0.449
Ni ₃	0.352	0.0	0.000	0.0	0.323	0.0	0.001	0.0	0.366
Ni ₄	0.449	0.0	-0.007	0.0	0.452	0.0	0.015	0.0	0.452
Ni ₅	0.437	0.0	0.005	0.0	0.446	0.0	-0.015	0.0	0.432
	L_A	L_B	L_C	L_A	L_B	L_C	L_A	L_B	L_C
Ni ₁	0.105	0.0	0.000	0.0	-0.085	0.0	0.009	0.0	0.080
Ni ₂	0.097	0.0	-0.010	0.0	-0.082	0.0	-0.012	0.0	0.093
Ni ₃	0.092	0.0	0.000	0.0	-0.065	0.0	0.001	0.0	0.060
Ni ₄	0.097	0.0	0.010	0.0	-0.088	0.0	-0.012	0.0	0.096
Ni ₅	0.105	0.0	-0.001	0.0	-0.092	0.0	-0.009	0.0	0.079

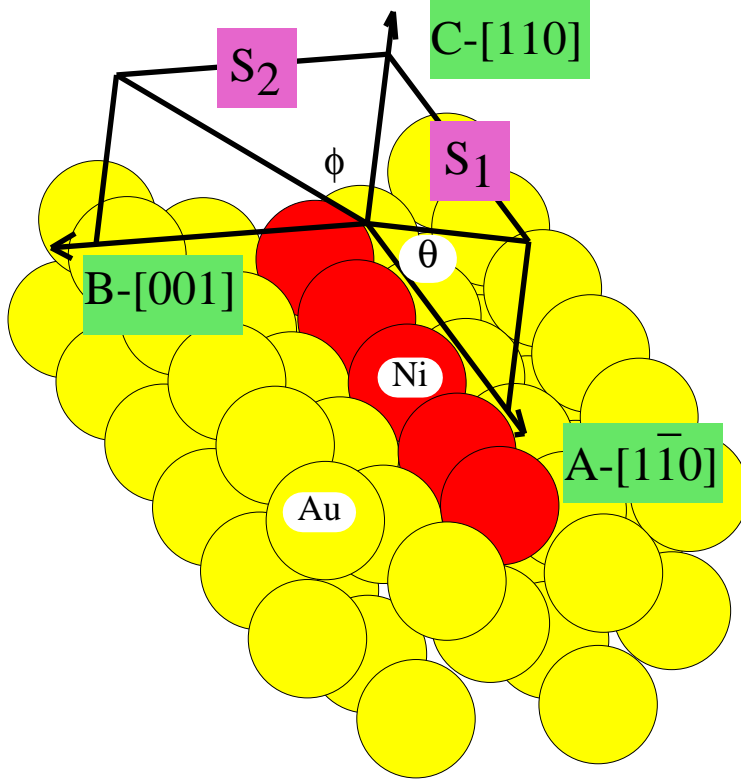
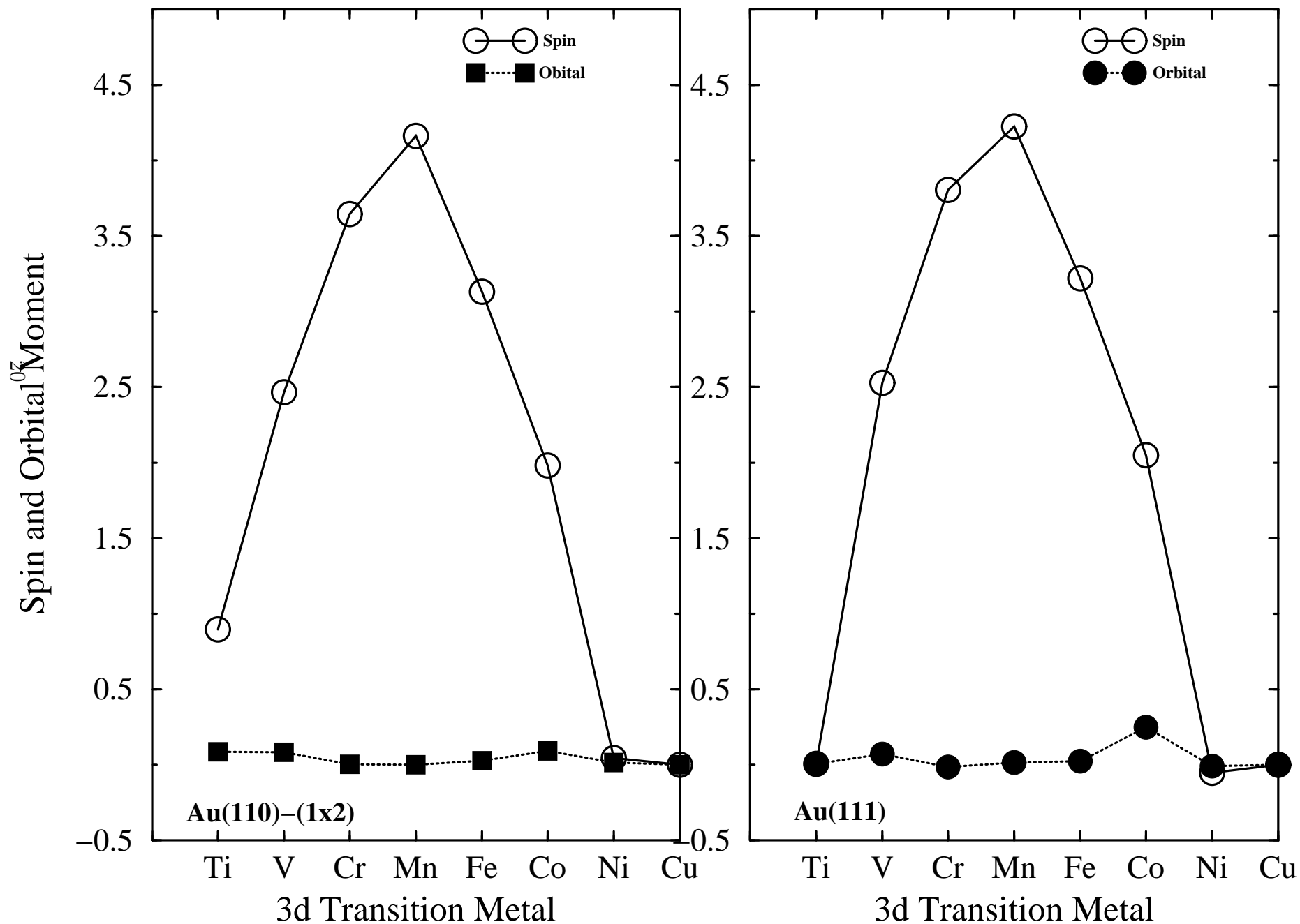


Fig. 1. The schematic diagram of a Ni chain supported on the Au(110)-(1 \times 2) surface. The trough of the reconstructed surface is along the A-[1 $\bar{1}$ 0] direction. The red spheres are the absorbed Ni atoms in the trough. The yellow spheres are the Au atoms of the surface. The plane including both C-[110] axis and A-[1 $\bar{1}$ 0] axis is named as S₁, the plane including both C-[110] axis and B-[001] axis as S₂. The rotating angle from any vector in S₁ to A-[1 $\bar{1}$ 0] axis labels as θ and the rotating angle from any vector in S₂ to C-[110] axis labels as ϕ . θ and ϕ are the magnetization angles in the two planes.

Fig. 2. The spin (solid lines) and orbital (dot lines) moments of the absorbed 3d atoms. The left panel shows the results for Au(110)-(1×2) surface, the right panel



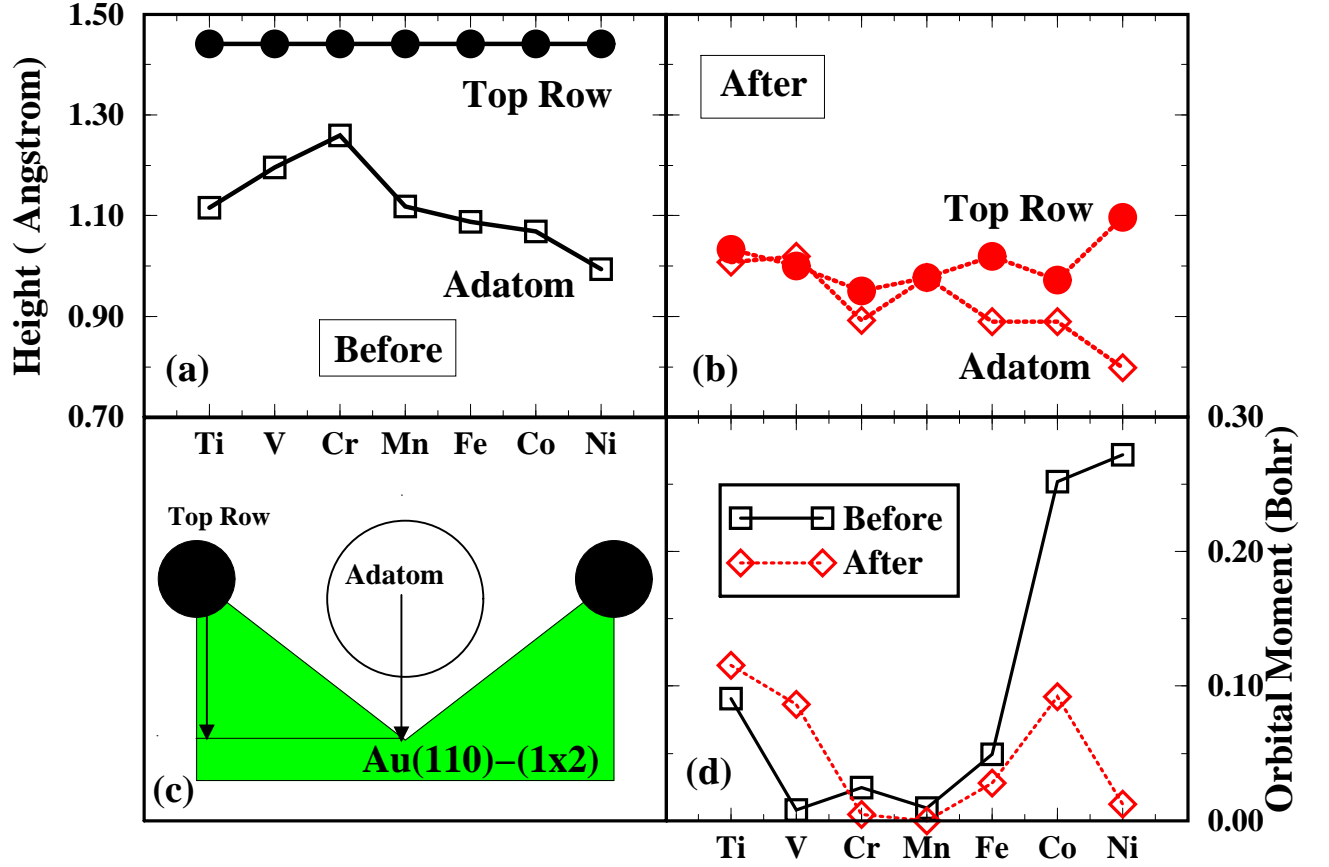


Fig. 3. The effects of structure-relaxation on orbital moments of the absorbed 3d transition metal atoms. (a). The heights of top-row and absorbed 3d atoms before the full-structure relaxations. The stable positions are different for different 3d atoms, which are obtained by the single-atom optimizations on the unrelaxed surface. (b). The heights of top row and absorbed 3d atoms after having done full-structure relaxations. The V atom is higher above the top row after the full-relaxation. (c). The schematic figure defines the heights of top row and absorbed atoms using two arrows pointing to the bottom of the trough. (d). The orbital moments change before and after the full-relaxations.

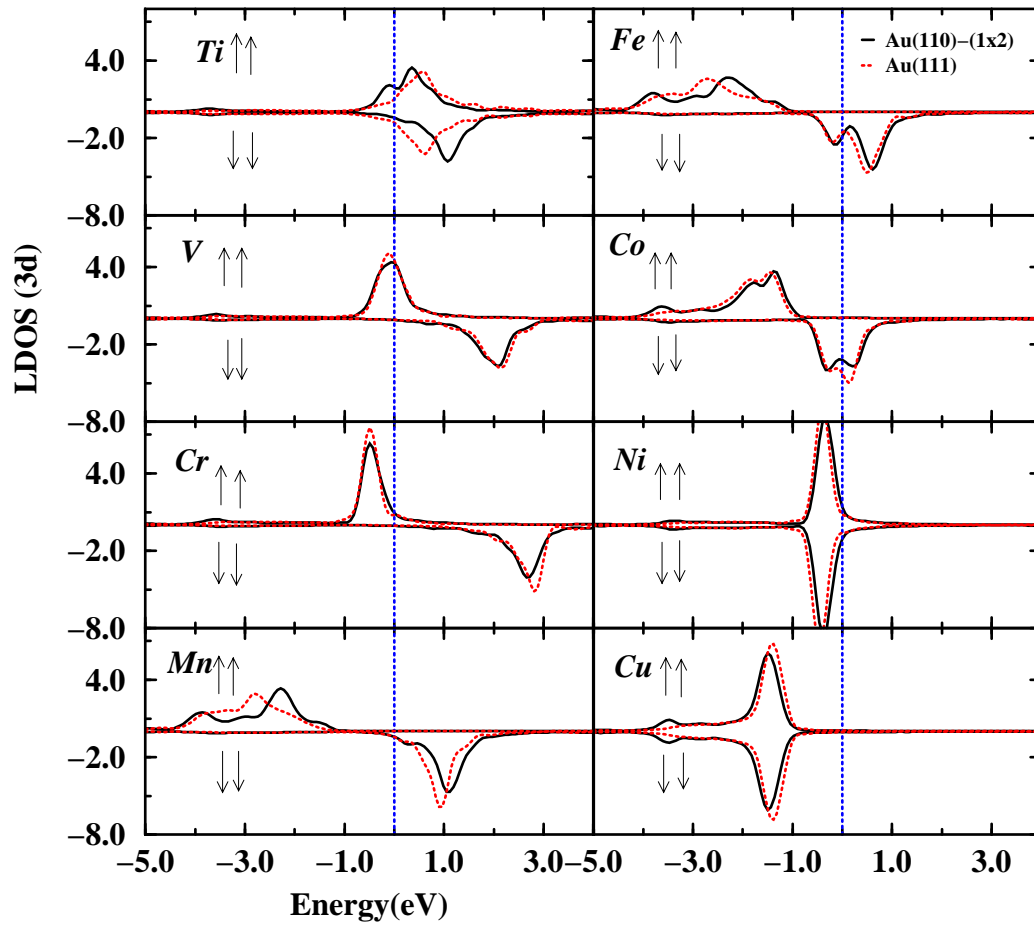


Fig. 4. The 3d densities of state (DOS) for the 3d atoms absorbed on Au(110)-(1 \times 2) (solid lines) and Au(111) (dot lines) surface.

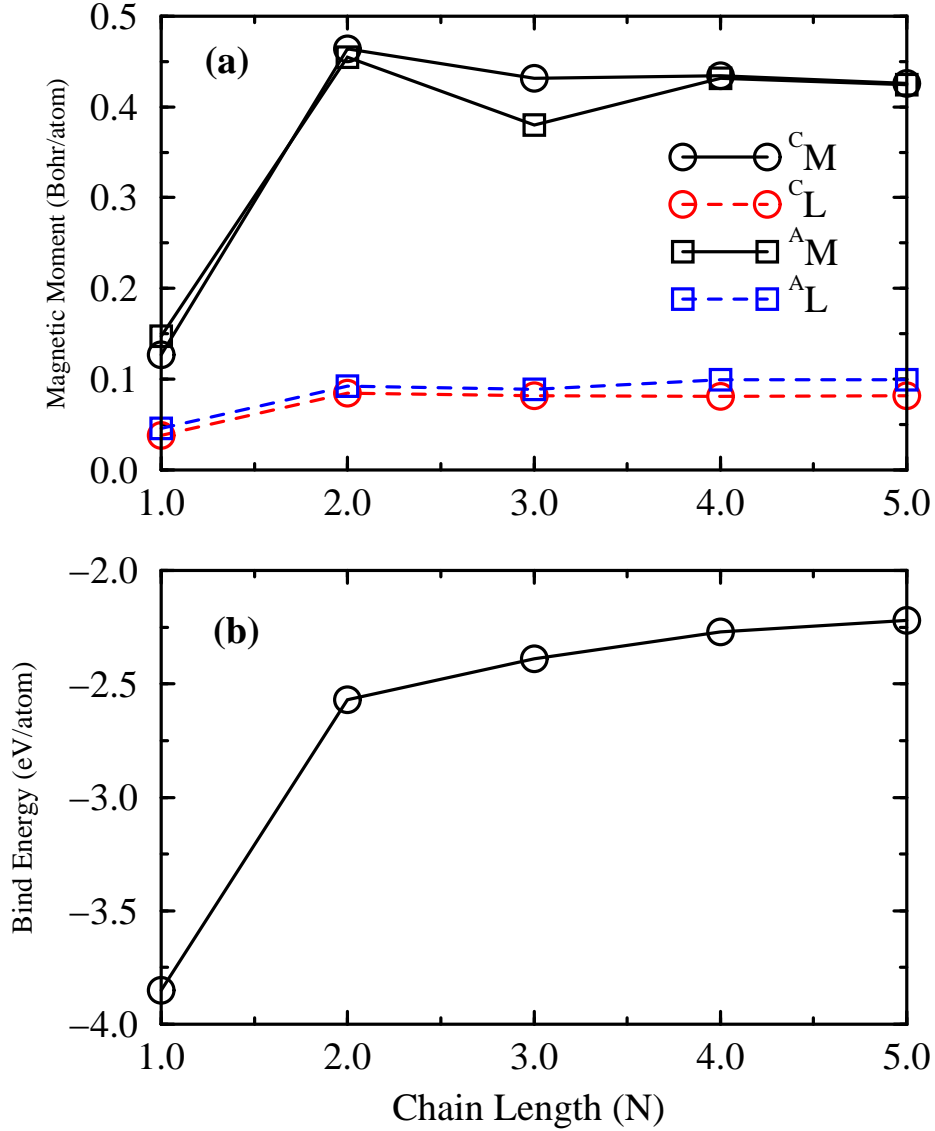


Fig. 5. (a) The spin $^A M$, $^C M$ and orbital $^A L$, $^C L$ moments change with the length of Ni chains. $^A M$ and $^C M$ aren't the A and B components of the spin moment \vec{M} . They are the spin magnetic moments when the magnetization along the A-[110] and C-[110] direction and are obtained from different self-consistent calculations. $^A L$ and $^C L$ have the same meaning for orbital moments. (b) Interaction energies between the Ni chains and the surface. The larger absolute values indicate the stronger interaction with the surface.

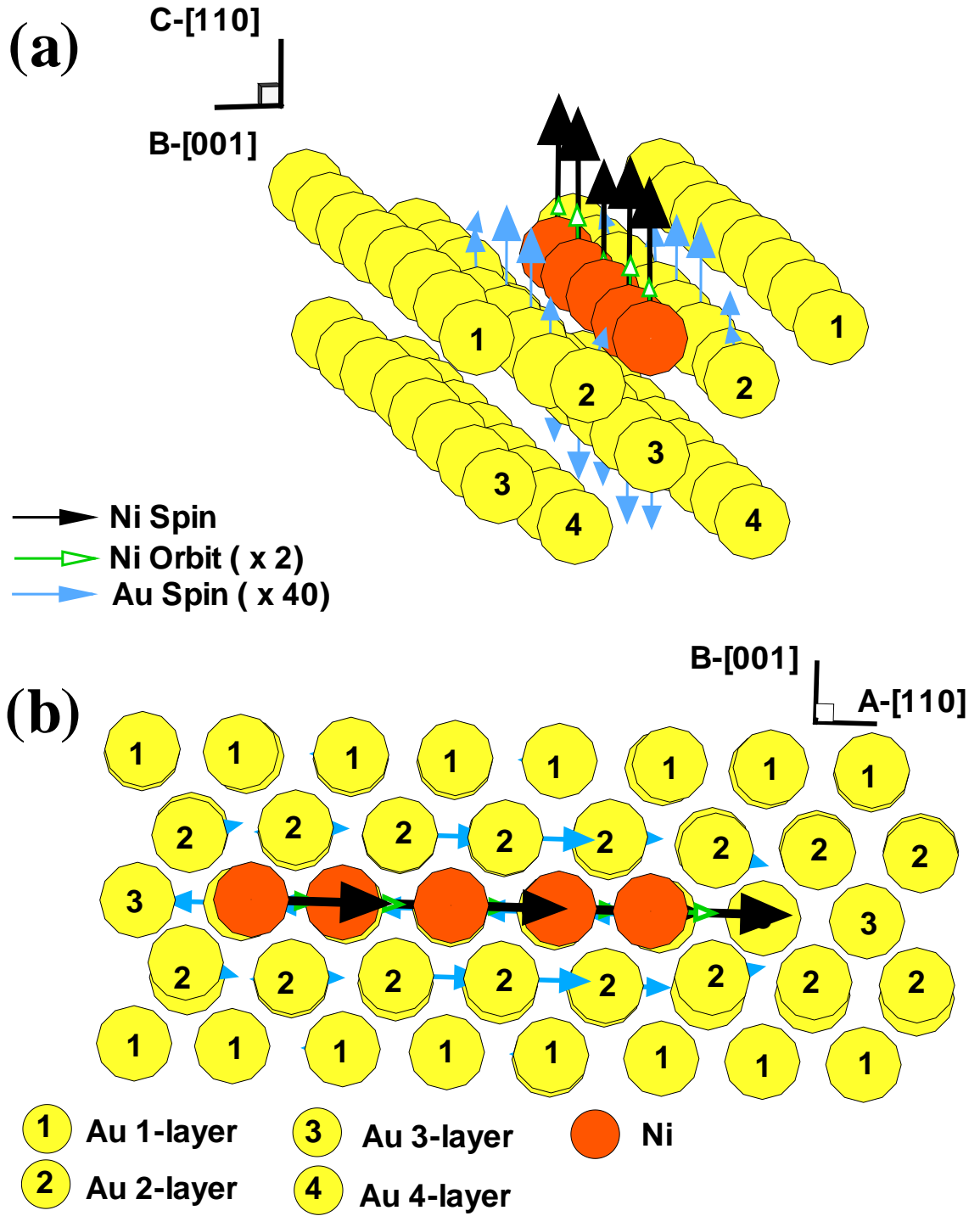


Fig. 6. The vector graph of the spin magnetic moments of the Ni chain which illustrates the ferromagnetic order of the Ni_5 chain based on our calculations. Especially, (a) and (b) are corresponding to the magnetization along $C-[110]$ and $A-[110]$ direction respectively. The smaller spin magnetic moments of Au atoms and the orbital magnetic moments of Ni atoms are multiplied by 40 and 2 respectively to show them with the larger spin moments of Ni atoms together in the same figure clearly.

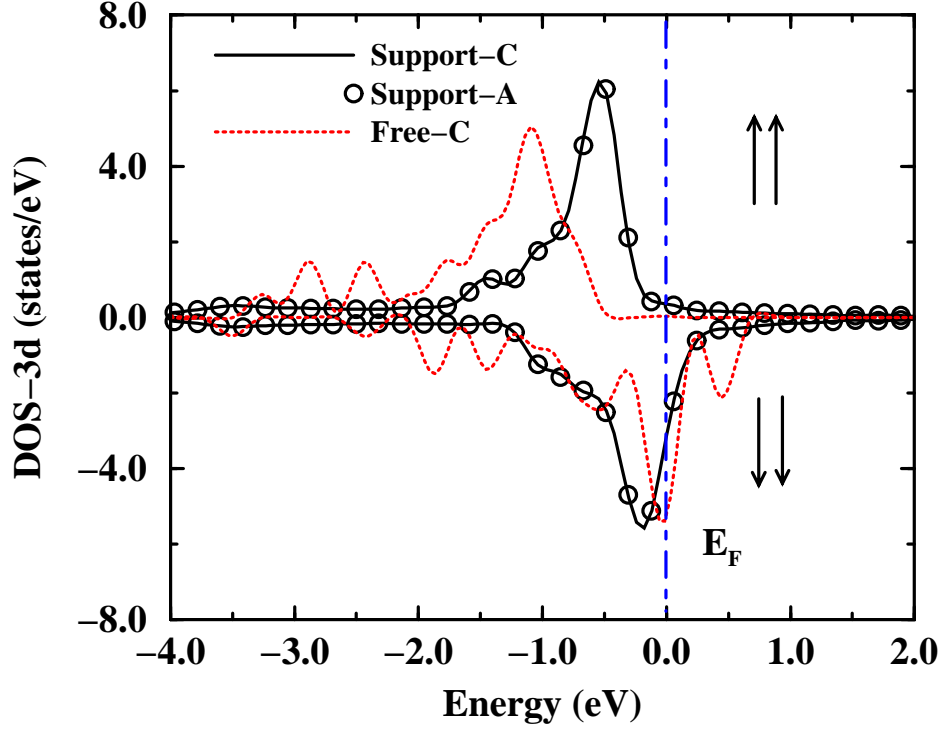


Fig. 7. The projected DOS of 3d states of the supported Ni_5 chain along the directions of magnetization when the chain is magnetized along different directions respectively (the solid lines for the C-[110] direction and the circles for the A-[$\bar{1}\bar{1}$ 0] direction). The spin-up (or spin-down) means along the positive (or negative) direction of two magnetization directions. This shows that spin degree of freedom is less relevant to magneto-crystalline anisotropy. The dots line is the DOS for free-standing Ni chain when magnetizing it along C-[110] direction.

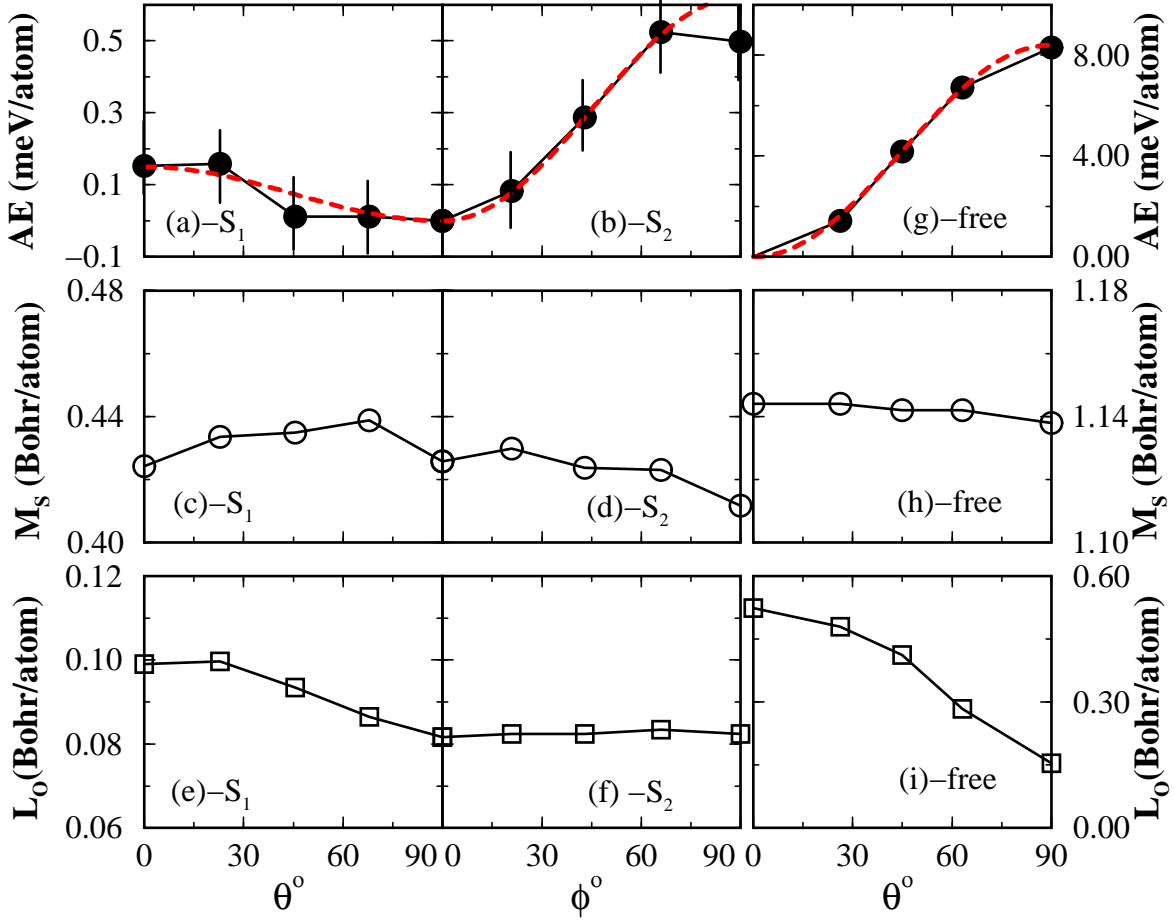


Fig. 8. The anisotropy energies (a,b), the spin (c,d) and orbital moment (e,f) of the supported Ni_5 chain change with the magnetization angles θ and ϕ in the planes S_1 and S_2 defined in above. The easy magnetization direction is perpendicular to the surface $\theta = 90^\circ$ and $\phi = 0^\circ$. The anisotropy energies (g), spin moment (h) and orbital moment (i) of the free standing Ni_5 chain change with the magnetization angles θ in the planes S_1 . The easy magnetization direction is parallel to the chain $\theta = 0^\circ$. Error bars in (a,b) represent the lowest limit of allowed error in total energy about ± 0.1 meV. The magnetic anisotropy energy curves are fitting using function $K_0 + K_1 \sin^2(\theta)$ for (a,g) and $K_0 + K_1 \sin^2(\phi)$ for (b)(red dash-lines).